01 Jan 2008

Shear Wave Splitting and Mantle Flow Associated with the Deflected Pacific Slab beneath Northeast Asia

Kelly H. Liu
Missouri University of Science and Technology, liukh@mst.edu

Stephen S. Gao
Missouri University of Science and Technology, sgao@mst.edu

Yuan Gao
Missouri University of Science and Technology

Jing Wu

Recommended Citation

K. H. Liu et al., "Shear Wave Splitting and Mantle Flow Associated with the Deflected Pacific Slab beneath Northeast Asia," *Journal of Geophysical Research*, vol. 113, no. B1, American Geophysical Union (AGU), Jan 2008.
The definitive version is available at https://doi.org/10.1029/2007JB005178

Shear wave splitting and mantle flow associated with the deflected Pacific slab beneath northeast Asia

Kelly H. Liu,[1] Stephen S. Gao,[1] Yuan Gao,[2] and Jing Wu[2]

Received 21 May 2007; revised 26 September 2007; accepted 18 October 2007; published 17 January 2008.

[1] A total of 361 *SKS* and five local *S* wave splitting measurements obtained at global and regional seismic network stations in NE China and Mongolia are used to infer the characteristics of mantle fabrics beneath northeast Asia. Fast polarization directions at most of the stations in the western part of the study area are found to be consistent with the strike of local geological features. The dominant fast directions at the eastern part, beneath which seismic tomography and receiver function studies revealed a deflected slab in the mantle transition zone (MTZ), are about 100° from north, which are almost exactly the same as the motion direction of the Eurasian plate relative to the Pacific plate, and are independent of the direction of local geological features. The splitting times at those stations are about 1 s which correspond to a layer of about 150 km thickness with a 3% anisotropy. The shear wave splitting observations, complemented by the well-established observation that most of the eastern part of the study area is underlain by a lithosphere thinned by delamination in the Paleozoic era, can be best explained by the preferred alignment of metastable olivine associated with the subduction of the deflected Pacific slab in the MTZ, or by back-arc asthenospheric flow in the mantle wedge above the slab.

Citation: Liu, K. H., S. S. Gao, Y. Gao, and J. Wu (2008), Shear wave splitting and mantle flow associated with the deflected Pacific slab beneath northeast Asia, *J. Geophys. Res.*, *113*, B01305, doi:10.1029/2007JB005178.

1. Introduction

[2] Polarization anisotropy determined by splitting of *P*-to-*S* converted waves at the core-mantle boundary has been increasingly used to infer finite strain caused by deformation in the mantle (see *Silver* [1996], *Savage* [1999], and *Fouch and Rondenay* [2006] for reviews). The two splitting parameters, fast polarization direction (ϕ) and the splitting time between the fast and slow waves (δt), are measures of the orientation and magnitude of mantle deformation, respectively. Observations of anisotropic textures in deformed mantle rocks and measurements of their seismic anisotropy have revealed that lattice preferred orientation (LPO) of crystallographic axes of olivine is the main cause of upper mantle anisotropy. Under uniaxial compression, the *a* axis of olivine, along which seismic *P* waves have the highest propagating velocity, rotates to be perpendicular to the maximum compressional strain direction; under pure shear, it becomes perpendicular to the shortening direction; and under progressive simple shear, it aligns in the flow direction [*Silver and Chan*, 1991].

[3] Numerous shear wave splitting measurements have been obtained in a back-arc environment, mostly in areas within a few hundred km from the trench. Because of the complicated mantle flow pattern above and below the slab in those areas, trench parallel, trench orthogonal, and trench oblique fast directions were observed [e.g., *Ando et al.*, 1983; *Bowman and Ando*, 1987; *Russo and Silver*, 1994; *Fischer et al.*, 1998; *Smith et al.*, 2001; *Anderson et al.*, 2004; *Audoine et al.*, 2004; *Baccheschi et al.*, 2007]. (See *Lassak et al.* [2006] for a discussion and modeling of the complexity.) A wide range of the depth of anisotropy was suggested, ranging from above the slab in the mantle wedge [*Fischer et al.*, 1998], inside the slab [*Sandvol and Ni*, 1997], and below the slab [*Russo and Silver*, 1994; *Baccheschi et al.*, 2007].

[4] This study is aimed at quantifying the orientation, magnitude and depth of mantle anisotropy beneath northeast Asia. Seismic tomography studies [*Fukao et al.*, 2001; *Miller et al.*, 2006; *Zhao et al.*, 2007] revealed that the eastern part of the study area is in the back-arc region of the Japan subduction zone, and is underlain by the horizontally deflected Pacific slab. The slab reaches about 600 km depth at a horizontal distance of approximately 1100 km from the trench, and is deflected horizontally in the MTZ to a distance of about 1900 km (Figure 1). Stacking of *P*-to-*S* converted phases from the top and bottom of the MTZ found a depressed 660 km discontinuity in the area occupied by the deflected slab, and that the top of the MTZ is at a depth of about 430 km [*Ai et al.*, 2003].

[5] While *SKS* splitting parameters have been previously obtained at most of the stations (Table 1), the current study is motivated by the following factors:

[6] 1. For most of the stations, results from the previous studies [*Silver and Chan*, 1991; *Zheng and Gao*, 1994;

[1]Department of Geological Sciences and Engineering, Missouri University Science and Technology, Rolla, Missouri, USA.
[2]Institute of Earthquake Sciences, China Earthquake Administration, Beijing, China.

0148-0227/08/2007JB005178$09.00

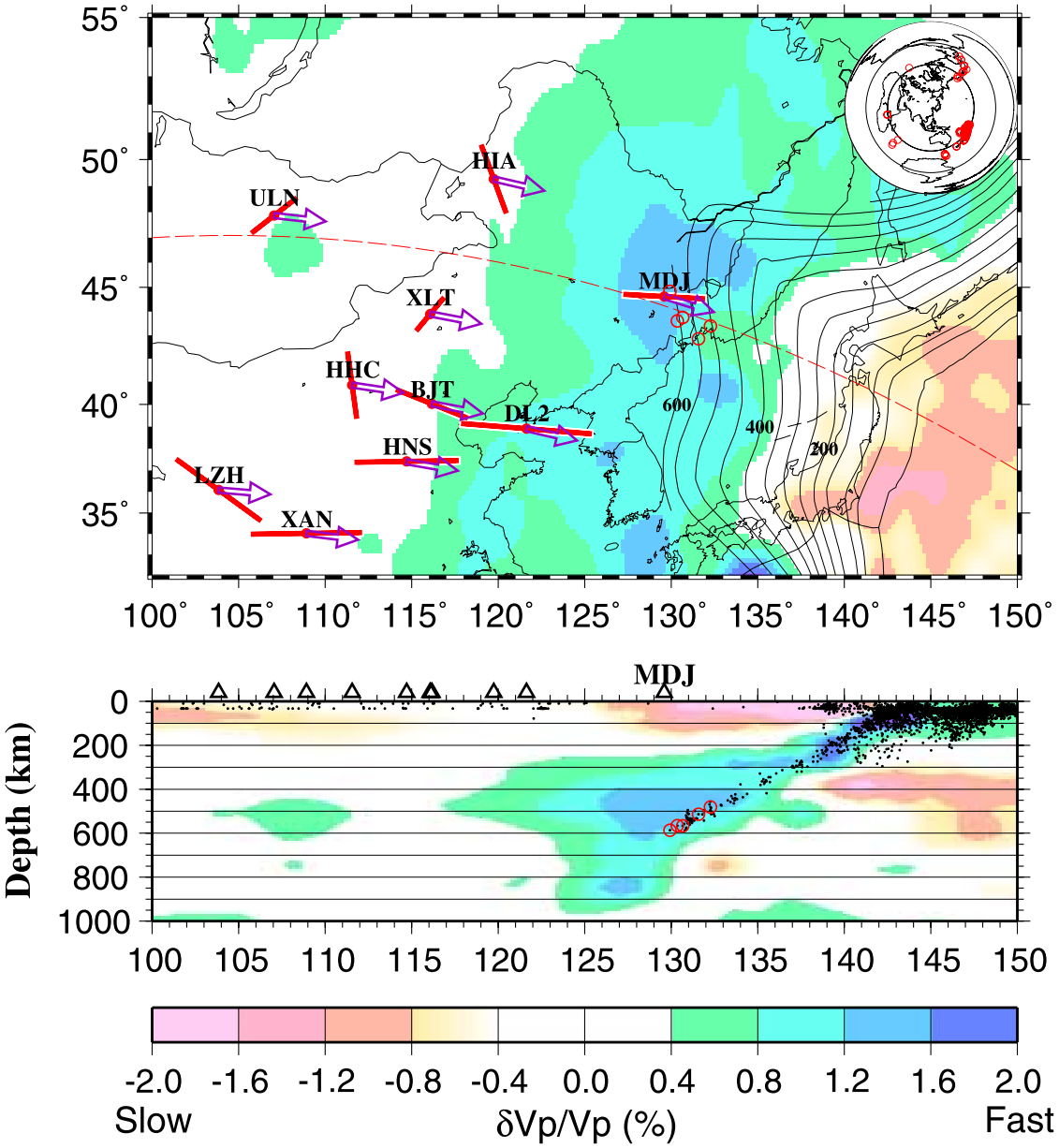

Figure 1. (top) Seismic velocity variation in the depth range of 397–670 km in the WEPP2 mantle model [*Fukao et al.*, 2001] and depth contours of the subducting Pacific slab. Solid bars represent the mean splitting parameters at each station, and open arrows show plate motion direction of Eurasia relative to the Pacific plate calculated based on the NUVEL-1 model [*DeMets et al.*, 1990]. Inset shows the 361 events used in the study. (bottom) A cross section along the dashed line in Figure 1 (top). Dots are magnitude 4.5 or larger earthquakes which occurred between 1963 and 2007 in the latitude range of 40°–45°. In both plots, circles are the five deep earthquakes used for splitting analysis of local *S* waves at MDJ.

Sandvol and Ni, 1997; *Iidaka and Niu*, 2001; *Liu et al.*, 2001; *Luo et al.*, 2004; *Zhao and Zheng*, 2005] are dramatically contradictory to each other in the resulting values of ϕ, δt, or both (Table 1). The inconsistency was mostly due to the limited number of events used for most of the stations by the previous studies, and to different *SKS* splitting measurement techniques and different data processing and selection criteria used by the studies. For most of the studies, information about the criteria of accepting or rejecting the measurements are not presented. We have realized that many excellent events were not, but some low-quality events were, used by some of the studies.

[7] 2. Reliable results from stations DL2, XLT, LZH which are critical for reaching the main conclusions of the study were not obtained.

[8] 3. The depth of the source of anisotropy was not constrained.

[9] 4. Discussions about the existence of complex anisotropy were absent.

Table 1. *SKS* Splitting Measurements From Previous and the Present Studies

Station (Latitude, Longitude)	ϕ	σ_ϕ	δt, s	$\sigma_{\delta t}$, s	N	Reference
BJT(40.02°, 116.17°)	110°	-	0.8	-	5	*Zheng and Gao* [1994]
	176°	36°	1.4	0.1	3	*Liu et al.* [2001]
	73°	3°	0.3	0.2	9	*Iidaka and Niu* [2001]
	104°	8°	0.9	0.1	30	*Luo et al.* [2004]
	59°	5°	0.9	0.1	6	*Zhao and Zheng* [2005]
	112°	10°	0.8	0.3	35	this study
DL2(38.91°, 121.63°)	95°	6°	1.5	0.4	3	this study
HHC(40.85°, 111.56°)	167°	7°	0.8	0.0	20	*Luo et al.* [2004]
	12°	1°	1.6	0.1	4	*Zhao and Zheng* [2005]
	172°	9°	0.7	0.1	27	this study
HIA(49.27°, 119.74°)	160°	5°	0.7	0.2	3	*Silver and Chan* [1991]
	160°	-	0.7	-	9	*Zheng and Gao* [1994]
	3°	8°	0.6	0.1	10	*Iidaka and Niu* [2001]
	124°	6°	1.2	0.1	16	*Liu et al.* [2001]
	159°	5°	0.8	0.0	36	*Luo et al.* [2004]
	160°	7°	0.8	0.1	78	this study
HNS(37.40°, 114.71°)	97°	12°	1.3	0.1	22	*Luo et al.* [2004]
	39°	2°	1.6	0.1	3	*Zhao and Zheng* [2005]
	89°	24°	1.1	0.5	16	this study
LZH(36.09°, 103.84°)	132°	4°	1.8	0.1	28	*Liu et al.* [2001]
	136°	45°	0.1	0.1	7	*Iidaka and Niu* [2001]
	126°	7°	1.2	0.3	6	this study
MDJ(44.62°, 129.59°)	118°	-	1.2	-	2	*Zheng and Gao* [1994]
	92°	19°	0.8	0.3	1	*Sandvol and Ni* [1997]
	95°	-	0.5	-	1	*Iidaka and Niu* [2001]
	140°	5°	1.5	0.2	5	*Liu et al.* [2001]
	103°	11°	1.2	0.3	11	*Luo et al.* [2004]
	93°	13°	0.9	0.3	18	this study
ULN(47.87°, 107.05°)	69°	6°	0.7	0.1	3	*Gao et al.* [1994b]
	45°	5°	1.4	0.4	9	*Luo et al.* [2004]
	52°	12°	0.6	0.1	89	this study
XAN(34.04°, 108.92°)	12°	9°	1.5	0.2	12	*Liu et al.* [2001]
	89°	5°	1.2	0.1	41	*Luo et al.* [2004]
	89°	4°	1.2	0.2	87	this study
XLT(43.90°, 116.08°)	40°	16°	0.5	0.0	2	this study

[10] This study measures *SKS* splitting parameters at permanent broadband stations in NE China and Mongolia. An objective procedure is developed and tested to rank the results. We infer the depth of the source of anisotropy using *S* waves from deep local earthquakes in the subduction zone, and discuss the possibility of complex anisotropy. Tectonically, the four stations located north of 43°N (ULN, HIA, XLT, and MDJ) are situated in the Mongolian Arcs Terrane, a Proterozoic-Paleozoic zone of arc and microcontinent accretion [*Kroner et al.*, 2005]. Five stations (HHC, BJT, DL2, HNS, and XAN) are on the Archean north China platform [*Ma et al.*, 1989; *Yin and Nie*, 1996; *Davis et al.*, 2001; *Darby et al.*, 2001]. Station LZH is on the E-W striking Qinling-Qilian orogenic belt which was created by collision between the north China and south China microplates during the Permian-Triassic time [*Ma et al.*, 1989; *Ren et al.*, 2002] (Figure 1).

2. Data and Method

[11] The broadband seismic data used in the study were recorded by 10 stations in China and Mongolia (Figure 2). Data from four of the stations (DL2, HHC, HNS, and XLT) were provided by the China Earthquake Administration (CEA) for the period of January 2001 to December 2004. The rest of the data set was recorded by stations in the China Digital Seismograph Network and the Global Seismographic Network, which are accessible from the Incorporated Research Institutions for Seismology (IRIS) Data Management Center (DMC). For *SKS* splitting measurements, we requested all the available broadband high-gain data from the IRIS DMC recorded by the six stations prior to (and including part of) 2006 from earthquakes of magnitude 5.8 or larger with an epicentral distance of 86° or greater. The recording duration ranges from about 20 years for HIA, LZH, and MDJ, 14 years for XAN, to about 10 years for BJT and ULN.

[12] The seismograms from both the CEA and IRIS stations were band-pass filtered in the 0.04 to 0.5 Hz range to improve signal-to-noise ratio (S/N). The *SKS* time window used to compute the splitting parameters is initially set as $a = 5$ s before and $f = 20$ s after the predicted *SKS* arrival times based on the IASP91 earth model. For events with an epicentral distance <90°, f is chosen as the theoretical arrival time of the direct *S* wave. We then visually check each of the seismograms to adjust the a and f values, and to reject the ones with strong non-*SKS* arrivals in the *SKS* window. The optimal pair of *SKS* splitting parameters (ϕ and δt) are obtained by searching for the one that minimizes the energy on the corrected transverse component. The errors in the resulting splitting parameters can be calculated using the inverse *F* test and represent the 95% confidence level (and are thus approximately 2 standard deviations) [*Silver and Chan*, 1991]. Figures 3 and 4 show examples of the original and corrected components for a station in the east, and a station in the west part of the study area, respectively.

3. Objective Ranking of Resulting Splitting Parameters

[13] A well-determined pair of splitting parameters is characterized by the clear *SKS* arrival on the original radial and transverse components, by the significant reduction of the *SKS* energy on the corrected transverse component, and by the small errors in the resulting ϕ and δt. Several conditions are necessary in order to obtain a well-defined pair of measurements, including (1) high S/N for presplitting *SKS* arrivals; (2) a large (>20°) difference between the back azimuth (BAZ) and the fast direction; and (3) strong azimuthal anisotropy with a horizontal axis of symmetry. Departure from one or more of the above conditions will lead to poorly determined results. In this study we objectively rank the resulting splitting parameters by using combinations of the following three parameters: (1) R_{or}, the signal-to-noise ratio on the original radial component, is a measure of the strength of the *SKS* signal; (2) R_{ot}, the signal- to-noise ratio on the original transverse component, is mostly related to the signal strength, magnitude of anisotropy, thickness of the anisotropic layer, and the angle between the fast direction and the arriving azimuth of the *SKS* raypath; and (3) R_{ct}, the signal-to-noise ratio on the corrected transverse component. Its ratio with R_{ot} is a measure of the significance of reduction of the energy on the corrected transverse component.

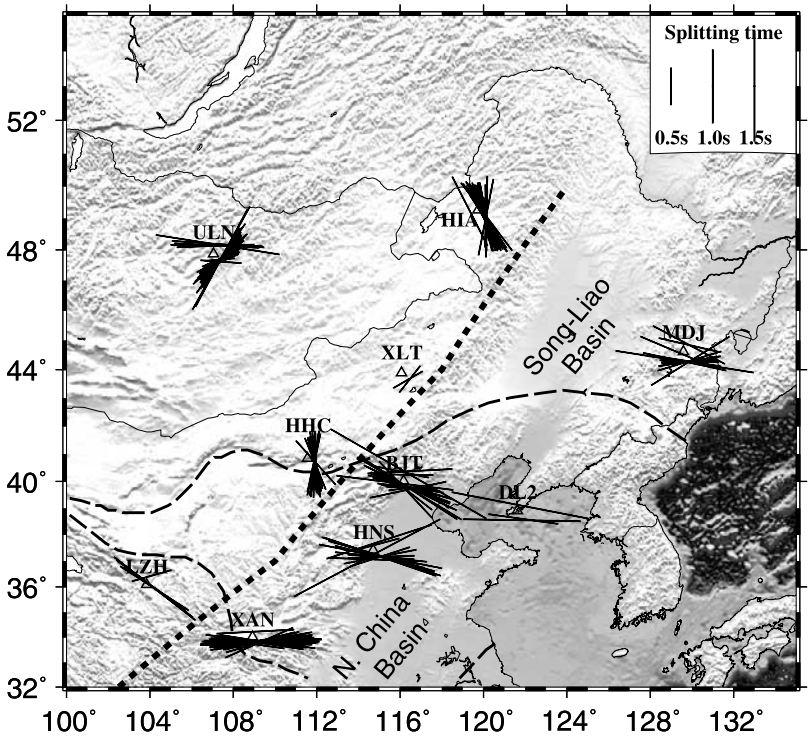

Figure 2. Map showing surface relief and individual *SKS* splitting measurements in the study area. The orientation of the bars, which are centered at the *SKS* ray-piercing points at 200 km deep, represents the fast polarization direction, and the length is proportional to the splitting time (see legend at the top right corner for scale). Triangles are stations used in the study. The thick dashed line indicates the boundary between the western and eastern regions of different characteristics of the observed anisotropy. The area between the thin dashed lines is the Archean north China platform, which is bordered by the Qinling-Qilian orogenic belt to the south and the Mongolian arcs terrane to the north [*Ren et al.*, 1999].

[14] The S/N is defined as

$$R = \frac{\max |A_{(a,f)}|}{\max |A_{(a-10,a)}|}, \quad (1)$$

where max $|A_{(a,f)}|$ is the maximum absolute value on the seismogram in the *SKS* time window between a and f, and max$|A_{(a-10,a)}|$ is the maximum absolute value on the seismogram in the time window between $a - 10$ s and a.

[15] The measurements are ranked into the following quality categories based on the R values (Figure 5):

[16] 1. Quality A is outstanding; $R_{or} \geq 10.0$, $R_{ot} \geq 2.0$, and $R_{ct}/R_{ot} \leq 0.7$. For a quality A measurement, outstanding energy on both the radial and transverse components is observed, and the measuring program was effective in reducing the energy on the transverse component.

[17] 2. Quality B is good; $3.0 \leq R_{or} < 10.0$, $R_{ot} \geq 2.0$, and $R_{ct}/R_{ot} \leq 0.7$. Seismograms used to obtain measurements in this category are similar to those in A, but with lower S/N on the radial component.

[18] 3. Quality N is null; $R_{or} \geq 3.0$, and $R_{ot} < 2.0$. The null measurements are the results of weak anisotropy, or the consequence of the *SKS* phase arriving from a direction that is close to the fast or slow directions. The null measurements are most useful to infer the nonexistence of anisotropy beneath a station, when null measurements are observed at two or more events with nonorthogonal different BAZs. Because clear splitting is observed at all the stations in the study area, the null measurements are not used in the discussion.

[19] 4. Quality S is special; $R_{or} \geq 3.0$, $R_{ot} \geq 2.0$, and $R_{ct}/R_{ot} > 0.7$. For measurements in this category, good or outstanding *SKS* arrivals can be observed on both the original radial and transverse components, but the energy on the corrected transverse component cannot be effectively reduced. For this study only about 4% of the measurements are in quality S and are mostly the result of some significant arrivals in the later portion of the *SKS* window. Most of the splitting parameters ranked as S are similar to those in quality A or B for the same stations.

[20] 5. Quality C is unusable; $R_{or} < 3.0$. Some of the measurements with quality A, B, or S are not well constrained as suggested by the large errors in ϕ or δt or both, and/or by the unreasonably large δt. Those measurements are also given a quality of C if $\sigma_{\phi} > 20°$, $\sigma_{\delta t} > 1.0$ s, or $\delta t > 2.5$ s. An upper limit of 2.5 s is chosen because splitting times of 2.5 s or larger are rarely observed on the continents [*Silver*, 1996]. Only A and B measurements are used in obtaining the station averages. Careful inspection of all the original and corrected seismograms suggests that the rank-

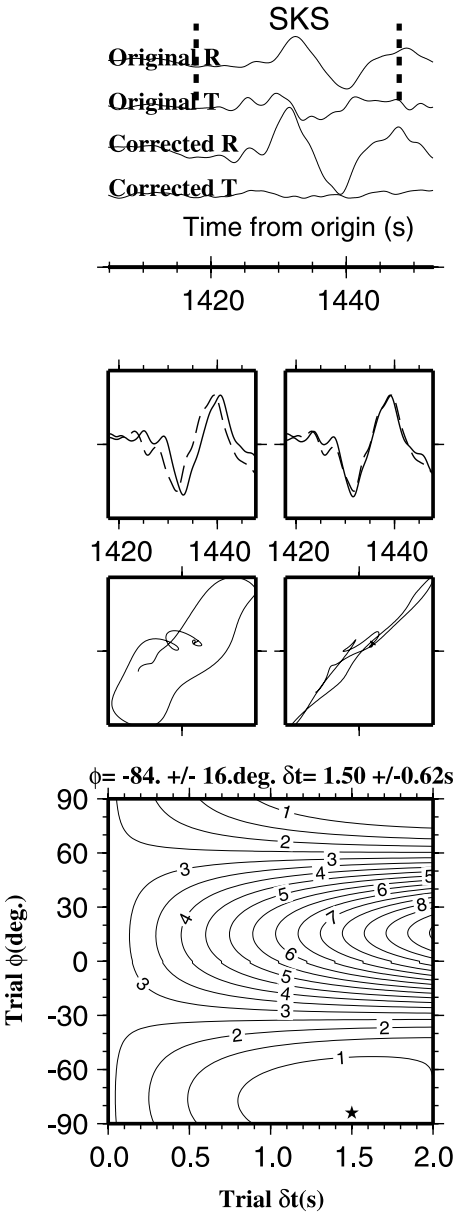

Figure 3. (top) Original and corrected *SKS* seismograms, (middle) particle motion patterns, and (bottom) contour map of the error function for an event recorded by station DL2. The measurement is ranked as quality B. The star in Figure 3 (bottom) marks the optimal splitting parameters.

ing procedure is robust and objectively reflects the quality of the measurements.

4. Shear Wave Splitting Observations

[21] A total of 751 measurements were obtained, of which 148 are quality A, 213 are B, 166 are C, 199 are N, and 25 are quality S measurements. Quality A or B (high-quality) splitting parameters of individual events are shown in Figure 2.

[22] The station average, $\bar{x}$, was computed from the N individual measurements weighted by the reciprocal of the variance obtained from the F test, i.e.,

$$\bar{x} = \left(\sum_{i=1}^{N} w_i x_i\right) \Big/ \sum_{i=1}^{N} w_i \tag{2}$$

where $w_i = 1/\sigma_i^2$, and x_i is the splitting parameter (ϕ or δt) for the ith event. The STD of $\bar{x}$ can be calculated using [*Zhang*, 2006]

$$\sigma_0 = \sqrt{\frac{1}{\sum_{i=1}^{N} w_i}} \tag{3}$$

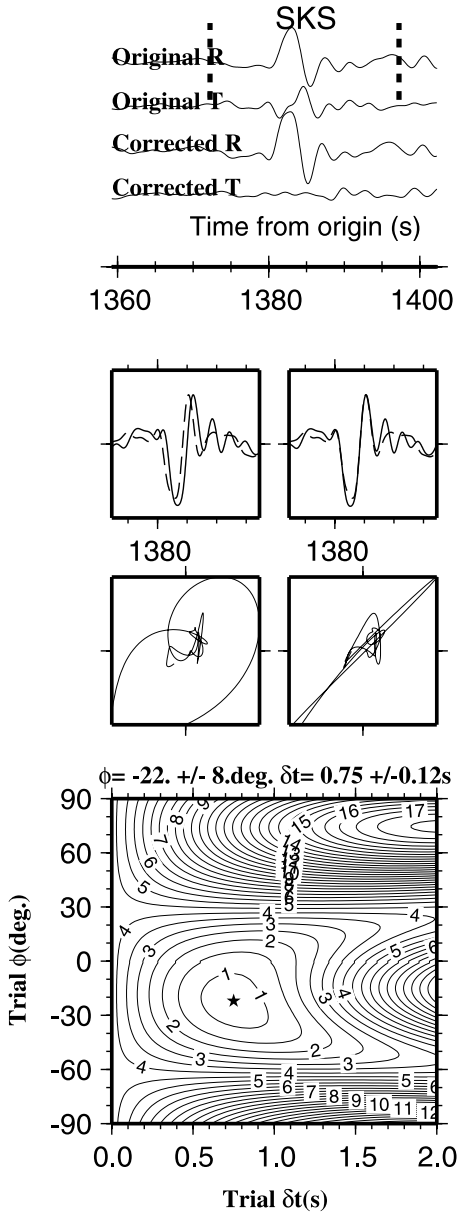

Figure 4. Same as Figure 3 but for station HHC. The measurement is ranked as quality A.

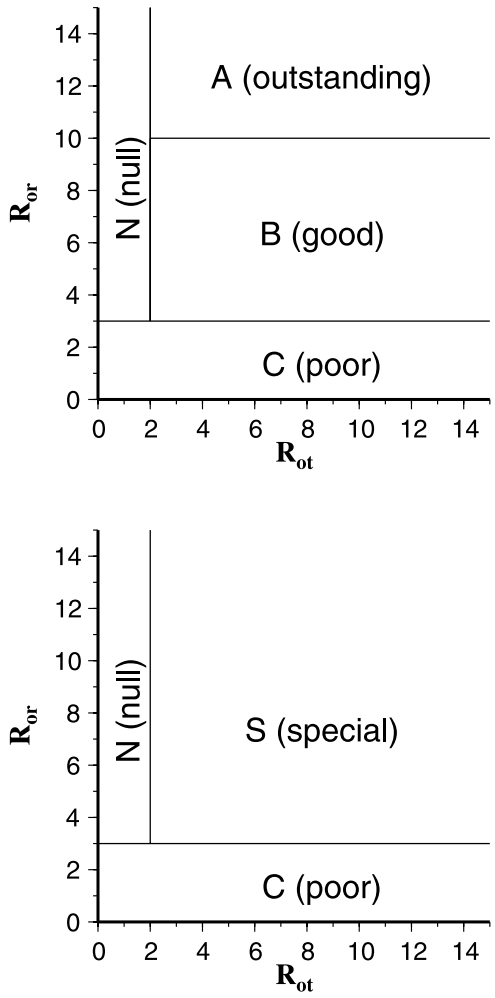

Figure 5. Diagrams used for objectively ranking the *SKS* splitting results. R_{or} is signal-to-noise ratio on the original radial component; R_{ot} is signal-to-noise ratio on the original transverse component. (top) For $R_{ct}/R_{ot} \leq 0.7$. (bottom) For $R_{ct}/R_{ot} > 0.7$, where R_{ct} is the S/N on the corrected transverse component.

which becomes $\sigma_0 = \sigma/\sqrt{N}$ when the individual measurements have the same STD. Some recent studies [e.g., *Zhang*, 2006] have found that the STD computed using equation (3) is always smaller than the true value. In addition, it cannot reflect the scattering of the splitting parameters with the back azimuth, angle of incidence [*Levin et al.*, 1999], frequency contents of the *SKS* waveform [*Ozalaybey and Chen*, 1999], and lateral heterogeneity of the degree and fast direction of anisotropy. Indeed, the STDs computed using equation (3) are unrealistically small, ranging from 0.2 to 3.8° and with a mean value of 1.1° for ϕ, and from 0.01 to 0.12 s with a mean of 0.04 s for δt. We thus used the unbiased estimator of sample STD as a measure of the degree of consistency among the individual measurements from a station, which is defined as [*Galassi et al.*, 2007]

$$\sigma_s = \sqrt{\frac{U_1 U_2}{U_1^2 - U_3}} \tag{4}$$

where $U_1 = \sum_{i=1}^{N} w_i$, $U_2 = \sum_{i=1}^{N} w_i (x_i - \bar{x})^2$, and $U_3 = \sum_{i=1}^{N} w_i^2$. Equation (4) becomes the more familiar form of

$$\sigma_s = \sqrt{\frac{1}{N-1} \sum_{i=1}^{N} (x_i - \bar{x})^2} \tag{5}$$

when the N samples are weighted equally. The STD values mentioned below and presented in Table 1 are sample STDs computed using equation (4).

[23] The study area can be divided into the western and eastern regions based on the characteristics of the observed splitting parameters. The boundary is approximately along the western edge of the Song-Liao and north China basins (Figure 2). Stations in the eastern region show almost uniformly E-W fast directions and comparable splitting times between 0.8 and 1.5 s. This corresponds to a layer of 120 to 220 km in thickness with a 3% anisotropy. Stations in the western region show spatially variable fast directions and splitting times, ranging from 0.5 s at XLT to 1.2 s at LZH.

4.1. BJT

[24] BJT (Baijiatuan, Beijing, China) is located on the north China platform, near the NW boundary of the late Mesozoic-Cenozoic north China basin and the NE-SW trending late Paleozoic-Mesozoic Yan-Shan fold belt [*Davis et al.*, 2001]. The strike of regional tectonic features is mostly NE [*Ma et al.*, 1989]. The mean splitting parameters from 35 high-quality measurements for BJT are (112 ± 10°, 0.8 ± 0.3 s). For this station, *Zheng and Gao* [1994] obtained (110°, 0.80 s) using five events, which is consistent with our result and those of *Luo et al.* [2004]. The results of *Iidaka and Niu* [2001], who obtained (73 ± 3°, 0.29 ± 0.17 s), *Zhao and Zheng* [2005], who reported a mean ϕ of 59 ± 5°, and *Liu et al.* [2001], who obtained (176 ± 36°, 1.4 ± 0.1 s), are contradictory to each other and to our results. Most of the high-quality events for BJT are from the SW Pacific subduction zone. Consequently, the existence of complex anisotropy for this station cannot be determined.

4.2. DL2

[25] Station DL2 (Dalian, Liaoning Province, China) is located on Precambrian basement rocks. The dominant strike direction of major basement faults in the vicinity of the station is NNE [*Ma et al.*, 1989]. Although all three measurements are ranked as quality B, the results from the events are statistically consistent, with a near E-W ϕ (95 ± 6°). The mean δt (1.5 ± 0.4 s) is the largest among all the stations.

4.3. HHC

[26] Station HHC (Huhehaote, Neimenggu Province, China) is situated on an approximately E-W striking Proterozoic orogenic belt [*Ma et al.*, 1989], the strike of which is almost orthogonal to the observed fast direction. All of the 27 events used to produce the high-quality measurements are from the SW Pacific subduction zone. The results (172 ± 9°, 0.7 ± 0.1 s) are statistically consistent with those of *Luo et al.* [2004], who reported (167 ± 7°, 0.8 ± 0.0 s), but are inconsistent with those of *Zhao and Zheng* [2005], who obtained (12 ± 1°, 1.6 ± 0.1 s).

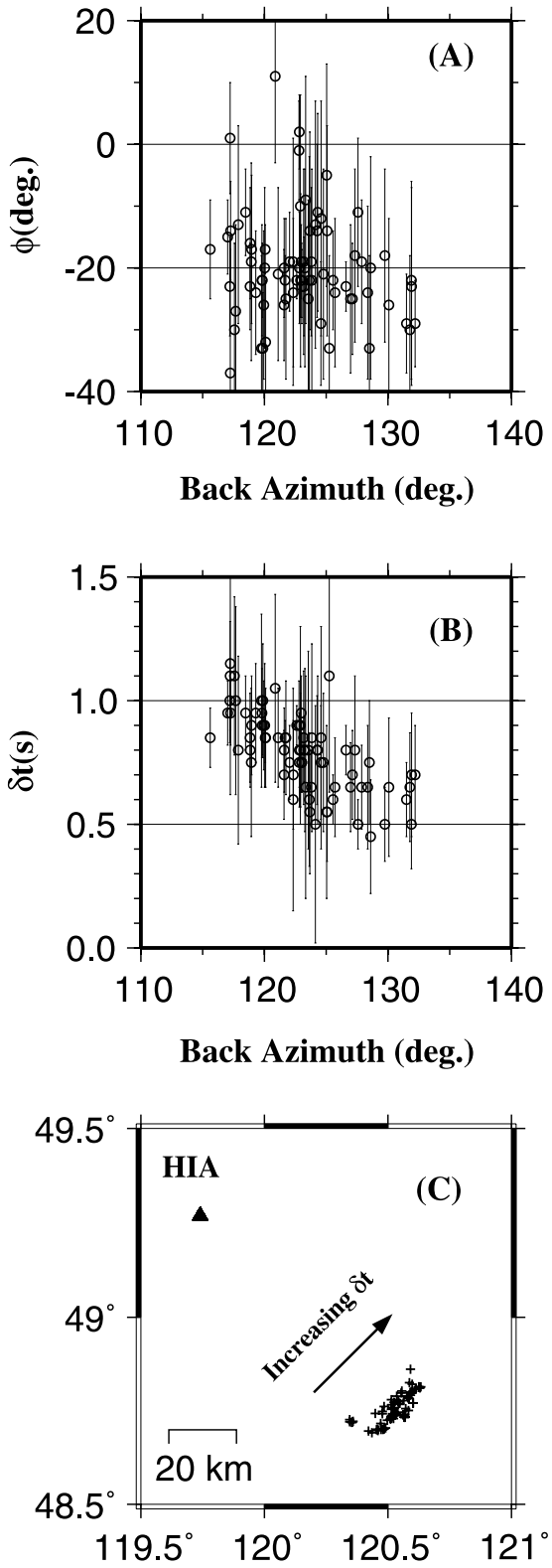

Figure 6. (a) Resulting ϕ and (b) δt measurements from events beneath the SW Pacific Ocean plotted as functions of back azimuth of the events for station HIA. Error bars represent 95% confidence interval from the *F* test. (c) Spatial distribution of *SKS* ray-piercing points at 400 km depth. The δt values increase toward the northeast.

4.4. HIA

[27] The strike of the Paleozoic orogenic belt on which station HIA (Hailar, Neimenggu Province, China) is situated is mostly NE-SW. Similar to HHC, the resulting ϕ observations from this study is nearly N-S (160 ± 7°), and the splitting time (0.8 ± 0.1 s) is among the smallest in the study area. Different *SKS* splitting results have been obtained at this station previously, including (1) (160 ± 5°, 0.7 ± 0.2 s) using 3 events [*Silver and Chan*, 1991]; (2) (160°, 0.7 s) using 9 events [*Zheng and Gao*, 1994]; (3) (159 ± 5°, 0.8 ± 0.0 s) using 36 events [*Luo et al.*, 2004]; (4) (3 ± 8°, 0.6 ± 0.1 s) using 10 events [*Iidaka and Niu*, 2001]; and (5) (124 ± 6°, 1.2 ± 0.1 s) using 16 events [*Liu et al.*, 2001]. Our results (160 ± 7, 0.8 ± 0.1 s) from 78 events are statistically consistent with the first three studies above.

[28] Except for one event located in the East African rift zone, all the other 77 events are from a narrow azimuthal zone with a back-azimuthal range of 116°−132°. The resulting δt measurements show a remarkable azimuthal dependence, from about 0.45 s to 1.15 s with a best fit slope of about −0.028 ± 0.003 s/degree (Figure 6). Such a statistically significant dependence is not observed for the ϕ values. The ray-piercing points at 400 km depth spread over a NE trending zone of about 25 km long.

[29] Under the assumption that the anisotropy is caused by a single layer with a horizontal axis of symmetry, the azimuthal dependence of the splitting times can be explained by a northeastward increase of the degree of anisotropy or the thickness of the anisotropy layer (or both) beneath the area sampled by the *SKS* phases (Figure 6c).

[30] An alternative cause of the azimuthal dependence is the existence of two-layer anisotropy [*Silver and Savage*, 1994]. We grid searched for the optimal pair of splitting parameters for the lower and upper layers, respectively, using the method of *Silver and Savage* [1994]. Like most previous determinations of splitting parameters under a two-layer anisotropy model, the resulting parameters are not well constrained and are statistically nonunique, mostly due to the limited azimuthal distribution of high-quality events. In the lack of a more comprehensive azimuthal coverage, our preferred model for the observed azimuthal dependence of δt at HIA is spatial variation of the magnitude of anisotropy and/or the thickness of the anisotropy layer. The lack of azimuthal dependence of the observed ϕ is consistent with this model. In addition, the eastward increase in δt can be explained by the increase in anisotropy associated with the subducting slab originated at the trench, which is located east of the station. Therefore this model is physically plausible.

4.5. HNS

[31] HNS (Hongshan, Hebei Province, China) is located in the SW boundary of the Mesozoic-Cenozoic north China basins, which were probably formed in a back-arc extension environment [*Ye et al.*, 1985; *Shedlock et al.*, 1985; *Gilder et al.*, 1991]. The major structures in the vicinity of the station are parallel to the NE-SW trending boundary of the basins. The 16 events recorded by HNS result in a mean δt of 1.1 ± 0.5 s and a mean ϕ of 89 ± 24°, which agrees with the strike of the major structures in the area. Our results are

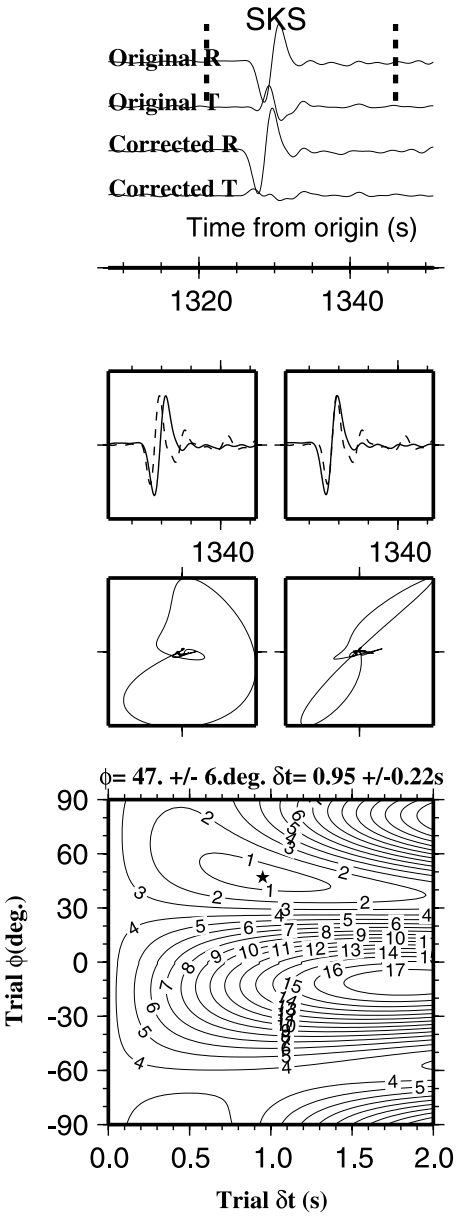

Figure 7. Same as Figure 3 but for station ULN.

consistent with those by *Luo et al.* [2004], but are significantly different from those obtained by *Zhao and Zheng* [2005], who used three events and obtained a ϕ of 39 ± 2° and a δt of 1.6 ± 0.1 s.

4.6. LZH

[32] Station LZH (Lanzhou, Gangsu Province, China) is located in the Qinling-Qilan fold belt, a WNW striking late Proterozoic–early Paleozoic orogenic zone [*Ma et al.*, 1989]. Weak anisotropy (0.14 ± 0.11 s) and unconstrained fast directions (136 ± 45°) were previously reported using 7 events occurred between 1990 and 1996 [*Iidaka and Niu*, 2001]. This is significantly different from our result of (126 ± 7°, 1.2 ± 0.3 s) using six events, five of which were originated from the southwest Pacific subduction zone and resulted in a fast direction ranging from 123° to 128° with a mean of 127 ± 3° which is parallel to the strike of the orogenic belt, and a splitting time ranging from 1.1 to 1.4 s with a mean of 1.2 ± 0.2 s. The other event, which was originated off the coast of northern California, resulted in a ϕ of 74 ± 18° and a δt of 0.55 ± 0.30 s. The azimuthal dependence of splitting parameters suggests either complex anisotropy or spatial variation of anisotropy in the vicinity of the station.

4.7. MDJ

[33] MDJ (Mudanjiang, Heilongjiang Province, China) is located in a Paleozoic orogenic belt between two NE-SW trending major active faults [*Ma et al.*, 1989; *Hsu and Chen*, 1999]. The mean splitting parameters for MDJ over 18 events are (93 ± 13°,0.9 ± 0.3 s), which are similar to the values of (118°, 1.2 s) of *Zheng and Gao* [1994] from 2 events, and to the results of (95°, 0.5 s) of *Iidaka and Niu* [2001] obtained using a single event. Our results are also consistent with those obtained by *Sandvol and Ni* [1997] using a single *SKS* event and with those by *Luo et al.* [2004] but are inconsistent with the results of (140 ± 5°, 1.5 ± 0.2 s) reported by *Liu et al.* [2001]. MDJ is the easternmost station and consequently, *S* waves from deep local earthquakes recorded by MDJ are used to constrain the depth of the source of seismic anisotropy, as described in section 5.1.

4.8. ULN

[34] The station is in the city of Ulaanbaatar, capital of Mongolia. The local strike of the Paleozoic-Mesozoic fold belt is NE-SW [*Ren et al.*, 2002]. A portable short-period (Mark Product 1 Hz L4C sensor) station was deployed in Ulaanbaatar for 5 months in 1992 as part of the Baikal rift seismic experiment [*Gao et al.*, 1994a] and a mean ϕ of 69 ± 6° and a δt of 0.7 ± 0.1 s were obtained using 3 events [*Gao et al.*, 1994b]. *Luo et al.* [2004] obtained a ϕ of 45 ± 5° and a δt of 1.4 ± 0.4 s using 9 events.

[35] When the original seismograms were used for *SKS* splitting measurements using the minimum transverse energy approach, which is used for all the stations in this study, most of the events show clear *SKS* energy on the corrected transverse component, and the resulting particle motion pattern is not linear (see Figure 7 for an example). When the criteria of minimizing the lesser of the two eigenvalues [*Silver and Chan*, 1991] is used, a linear particle motion pattern is achieved (Figure 8). The results from the two approaches are often statistically different for the same events recorded by ULN.

[36] The energy on the transverse component can be successfully minimized after the horizontal components are rotated by 10° clockwise before they are used for splitting measurements (Figure 9). All the seismograms recorded since the initial deployment of the station in 1990 need such a rotation in order to minimize energy on the corrected transverse component. The most likely cause of this observation is that the seismometer has been misoriented by 10°.

[37] The reason of such a misorientation is unclear. One possibility is that the local magnetic field at the site is disturbed so that the magnetic declination was significantly different from the expected value. Another possibility is that the sign of the declination (which is about 3.5–4.0° toward the west from 1995 to 2006 based on data from the National Geophysical Data Center) was mistaken, and as a result, the

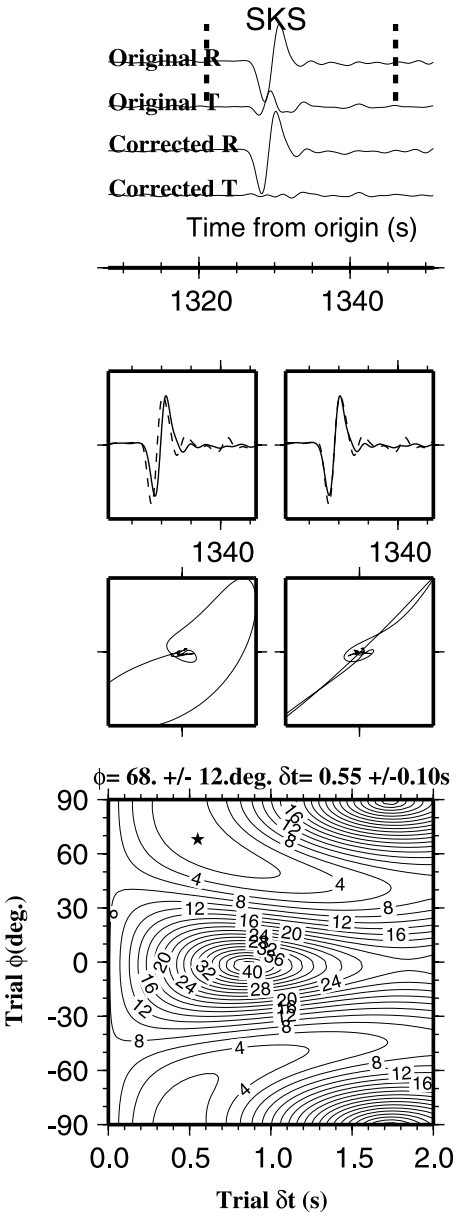

Figure 8. Same as Figure 7, but the minimum eigenvalue approach is used instead of the least transverse energy method.

seismometer was rotated 5 or so degrees counterclockwise instead of clockwise relative to magnetic north. The ϕ of 45° obtained by *Luo et al.* [2004] might be the result of the misorientation of the sensors.

[38] The 89 events can be divided into two groups based on the back azimuths. The first group has a BAZ between 21 and 34° with nearly E-W fast directions, and the second group has a BAZ in the range of 108–125° with mostly NE-SW fast directions. The narrow width of the BAZ bands prevents a unique determination of splitting parameters using a two-layer model. As a matter of fact, a two-layer model, which predicts 90° periodicity with regard to BAZ, is unlike to explain the apparent difference in the fast directions between the two groups, because the modulo-90° BAZ range for the second group is 18–35° which almost exactly overlaps with the BAZ of the first group. Therefore the most likely cause of the azimuthal dependence of the splitting parameters is lateral variation in the direction and strength of seismic anisotropy.

[39] The 89 quality A or B events (after the sensor alignment correction) resulted in a mean δt of 0.6 ± 0.1 s and a ϕ of 52 ± 12°, which is parallel to the strike of the Mongolian fold belt in this area.

4.9. XAN

[40] XAN (Xian, Shaanxi Province, China) is situated inside the seismically active Shanxi Graben, near the approximately E-W trending southern boundary. It is about 100 km west of the estimated epicenter of the 1556

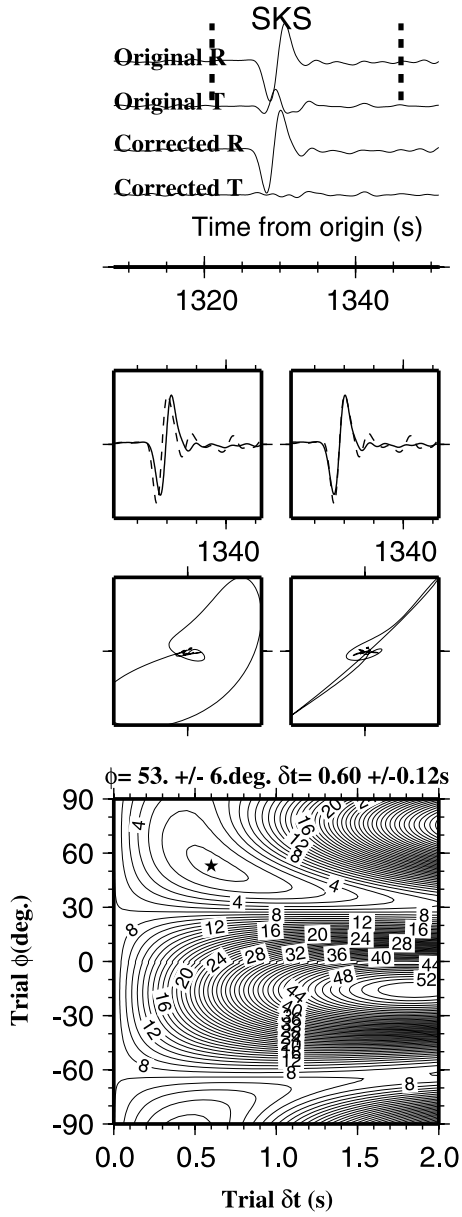

Figure 9. Same as Figure 7, but the horizontal components were rotated 10° clockwise prior to calculation of splitting parameters using the least transverse energy approach.

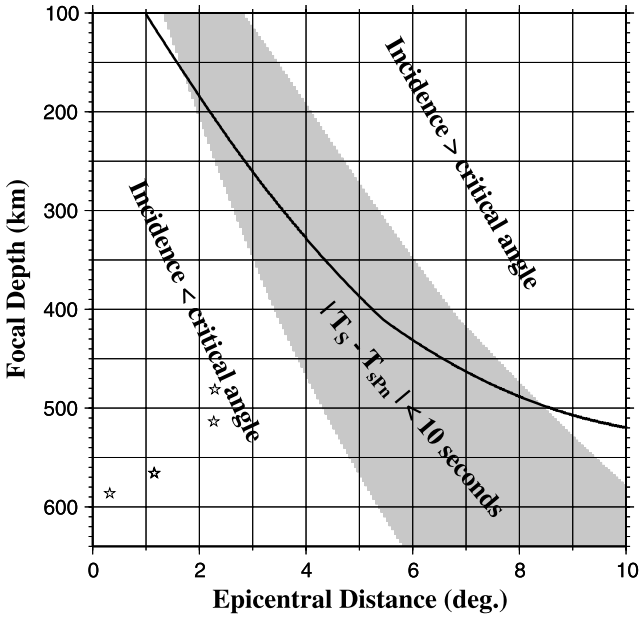

Figure 10. Results of theoretical calculations (based on the IASP91 Earth model) for the selection of local events suitable for shear wave splitting analysis. The *sPn* phase arrives 10 s or less before or after the arrival of the local *S* wave for events in the shaded area. The solid line presents events with a critical *S* wave angle of incidence (about 35°). Only events in the area on the left side of both the solid line and the shaded area are suitable for shear wave splitting analysis. Stars represent the five events used in the study (Table 2). Note that the two events with a depth of about 565 km almost overlap with each other.

magnitude 8 earthquake which caused estimated casualties of 830,000 [*He*, 1990]. Averaging over the 87 events recorded at XAN results in a ϕ of 89 ± 4°, which is parallel to the southern boundary of the graben, and a δt of 1.2 ± 0.2 s. The results are consistent with those of *Luo et al.* [2004] using 41 events, but are inconsistent with the results of *Liu et al.* [2001].

4.10. XLT

[41] In the vicinity of XLT (Xilinhaote, Neimenggu Province, China), the late Paleozoic orogenic belt where the station is located has a nearly E-W strike [*Ma et al.*, 1989]. Only two events from XLT are available for *SKS* splitting measurements, and they produced statistically consistent results for both ϕ (38 ± 5°, 60 ± 17°) and δt (0.45 ± 0.2 s, 0.45 ± 0.2 s). The large uncertainties in the observed ϕ values, which resulted in a mean of 40 ± 16°, are most likely the consequence of weak anisotropy, as XLT has the smallest δt in the study area.

5. Discussion

5.1. Constraints on the Depth Distribution of Anisotropy

[42] While *SKS* splitting measurements can place a reasonable constraint on the lateral location of the source of anisotropy, their resolving power on the depth of the source is low [*Marone and Romanowicz*, 2007]. From a pure wave propagation point of view, the source could be located anywhere along the raypath from the core-mantle boundary to the surface of the earth. When the seismic stations are closely spaced, spatial variations of the splitting parameters can provide some constraints on the depth of the anisotropic region(s), by comparing the observed horizontal span of consistent splitting parameters and the calculated size of the first Fresnel zone at various depth [*Alsina and Snieder*, 1996; *Rumpker and Ryberg*, 2000]. The stations that we used are hundreds of km apart and are thus not suitable for depth determination using the Fresnel zone approach.

[43] For stations that are close to the epicenter of deep earthquakes, vertical distribution of seismic anisotropy can be constrained by measuring splitting times from *S* waves of local events with different focal depths [e.g., *Ando et al.*, 1983]. In order to minimize the distortion of waveform due to strong interaction of the *S* wave with the free surface, only events within the *S* wave window, which is defined as the cone-shaped volume centered at the station, within which the *S* wave angle of incidence is $\sin^{-1}(V_s/V_p)$ or smaller, should be used for the analysis (Figure 10) [*Crampin and Booth*, 1985].

[44] In addition, *S* waves from events with a certain combination of focal depth and epicentral distance can be strongly distorted by the *sPn* phase, which is a *S*-to-*P* converted phase at the Moho and travels as a refracted wave along the top of the mantle (Figure 10). The angle of incidence of the *sPn* phase is large enough for the phase to be recorded at significant amplitudes by the horizontal sensors. For instance, the ray parameter of an *sPn* phase from an event of 500 km deep and 6° away is about 13.75 s/deg, which corresponds to an incidence angle (measured from the vertical) of about 46°, suggesting that the *sPn* phase will be recorded by the horizontal and vertical sensors with equal amplitudes. Our tests show that unrealistic (e.g., anomalously large δt) and unstable (in terms of the beginning and end of the time window used for analysis) results are frequently obtained if events outside the suitable window are used.

[45] Given the spatial distributions of the stations and local seismicity, only station MDJ is favorably located for local *S* wave splitting measurements. We search for magnitude $\geq$ 5.0 events with a focal depth $\geq$ 100 km within the suitable window (Figure 10) and found that a total of five such earthquakes that occurred prior to 2006 are available at the IRIS DMC. All of the events have a magnitude of 6.0 or greater, and the focal depths are in the range of 481 to 586 km (Figure 1 and Table 2). The seismograms are bandpass filtered between 0.05 and 1.0 Hz to enhance the S/N. We then apply the method of *Silver and Chan* [1991] to search for the optimal splitting parameters, which corresponds to the minimum of the smaller of the two eigenvalues of the covariance matrix computed from the rotated and shifted horizontal components. The resulting optimal parameters lead to the maximum linearity in the corrected particle motion. Figures 11 and 12 show examples of *S* wave waveform and results of splitting analyses. The fast directions from four of the five events are well defined and are nearly E-W, which is consistent with the fast directions from the *SKS* phase (Tables 1 and 2). One of the events (event 5) which is the shallowest and has the smallest δt (0.4 s), gives a poorly defined ϕ of 142 ± 18°, which is

Table 2. Individual *S* Splitting Measurements

Event	Time year-day UT	Latitude, deg	Longitude, deg	Depth, km	Magnitude	ϕ, deg	δt, s	BAZ deg	Δ, deg
1	99-098 1310	43.61	130.35	565	7.1	90 ± 2	1.3 ± 0.1	151	1.15
2	00-044 0257	42.85	131.57	513	6.0	81 ± 10	0.4 ± 0.1	140	2.27
3	02-179 1719	43.75	130.67	566	7.3	93 ± 4	1.1 ± 0.2	138	1.16
4	02-258 0839	44.83	129.92	586	6.4	89 ± 3	0.9 ± 0.1	47	0.32
5	03-243 2308	43.39	132.27	481	6.2	142 ± 18	0.4 ± 0.1	121	2.29

likely the consequence of weak anisotropy. The small error bars for most of the measurements (Table 2) are the results of the sharp waveform of the deep events, the very high signal-to-noise ratio, and the high linearity of the corrected particle motion patterns (Figures 11 and 12).

[46] Using *S* waves recorded by MDJ from three local events which occurred in 1992 and 1993, *Sandvol and Ni* [1997] found that the fast directions range from 53° to 90°, and the δt values vary from 1.0 to 2.2 s. The magnitude of two of the three events used by *Sandvol and Ni* [1997] is lower than the cutoff magnitude (5.0) that we used. The third event, which is a magnitude 6.6 earthquake with a focal depth of 448 km and an epicentral distance of 6.6° from MDJ, is outside the suitable zone (Figure 10). Thus the anomalously large δt (2.2 s) could be the result of waveform distortion by the *sPn* phase, which arrived about 4.5 s before the *S* wave.

[47] The resulting δt values show a statistically significant dependence on the focal depths, with a best fitting slope of 0.85 ± 0.13 s per 100 km (Figure 13). The splitting times obtained using *S* waves from the three deepest local events and those from the teleseismic *SKS* phases are comparable, suggesting that anisotropy in the mantle below about 600 km depth is insignificant along the *SKS* raypath. This is similar to the conclusion in other subduction zones such as Tonga [*Fischer and Wiens*, 1996]. In addition, the best fit relation between focal depths and splitting times suggests that beneath MDJ, the splitting time reduces to zero at a depth of about 440 km, which is close to the depth of the 410 km discontinuity in this area [*Ai et al.*, 2003]. The depth variation of the splitting times is consistent with a layer in the 440–590 depth range with a 3% anisotropy, a conclusion that is consistent with that of *Sandvol and Ni* [1997].

[48] It must be mentioned that the conclusion about the depth distribution of the source of anisotropy in the study area is based on a limited number of measurements and therefore might not be sustainable when additional high-quality observations from local earthquakes are added to the plot. An alternative interpretation of the apparent focal depth dependence of the *S* wave splitting times (Figure 13) is spatial variation of the magnitude of anisotropy in the area sampled by the *S* waves. The existence of rapid spatial variation in the degree of anisotropy beneath the study area is supported by the distribution of δt values observed at station HIA (Figure 6). If the alternative interpretation is true, the observed depth dependence of splitting times is simply a coincidence, and the depth of anisotropy remains undetermined, like the majority of other *SKS* splitting studies. Indeed, most studies in other subduction zones suggested insignificant depth variation of splitting times [e.g., *Fischer and Wiens*, 1996; *Fouch and Fischer*, 1996].

5.2. Cause of Observed Anisotropy: Lithospheric Deformation or Mantle Flow?

[49] Over the past decade the origin of mantle anisotropy has been a debated topic. On the basis of the observation that most fast directions are parallel to the regional tectonic trend of surface geological features, several authors proposed that at least in some areas, mantle anisotropy is

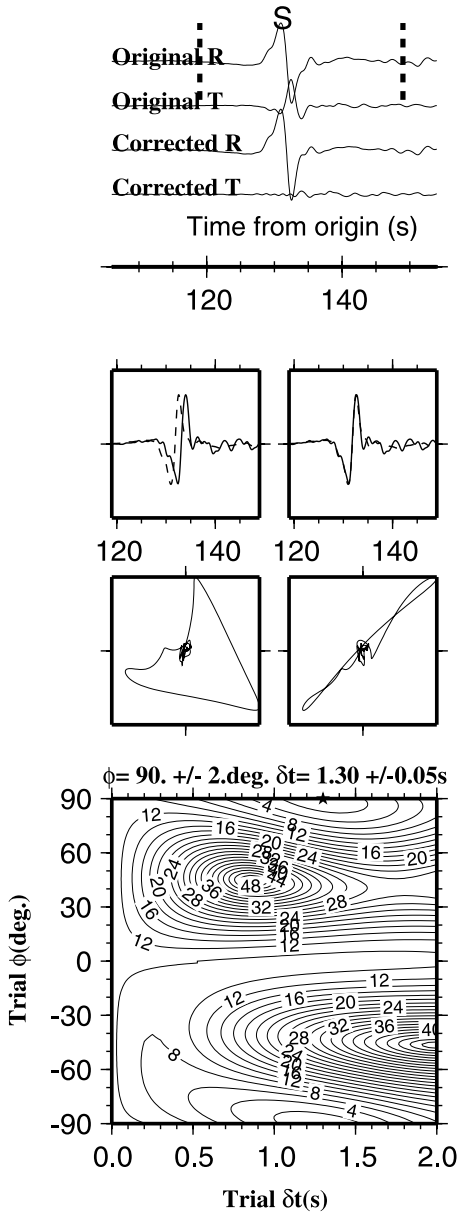

Figure 11. MDJ *S* wave splitting results from event 1 (Table 2), which has a focal depth of 565 km.

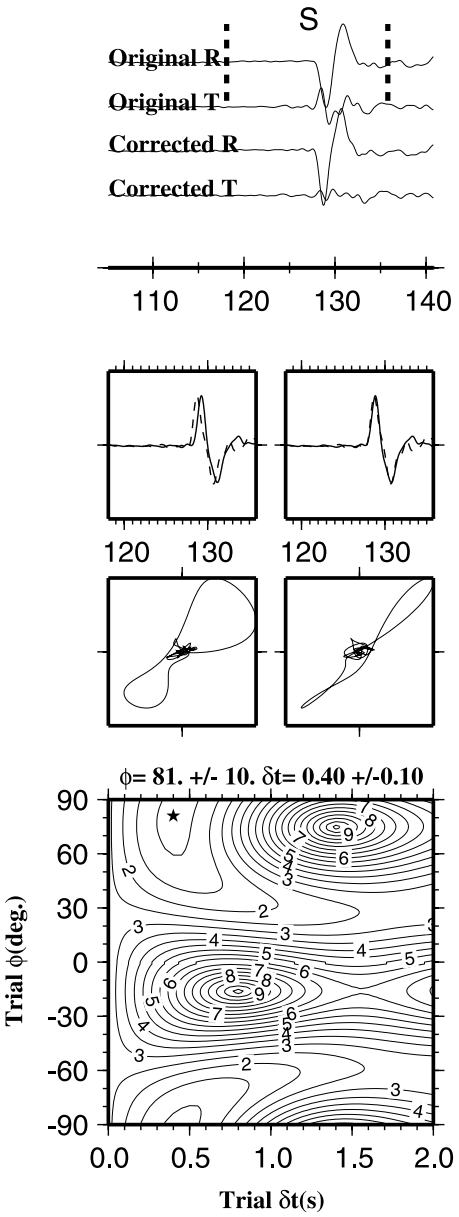

Figure 12. MDJ *S* wave splitting results from event 2, which is shallower (513 km) than event 1 and resulted in a smaller δt.

caused by coherent deformation of the lithosphere [e.g., *Silver and Chan*, 1991; *Liu et al.*, 1995; *Silver*, 1996; *Silver et al.*, 2001]. While this model can satisfactorily explain the anisotropy observed at stations ULN, LZH, and perhaps XAN, at which the strike of regional tectonics is consistent with the observed ϕ, it cannot account for the approximately uniform E-W fast directions observed in the eastern part of the study area, in which the strike of the tectonic features is mostly NE-SW. It also cannot explain the nearly N-S fast direction at HHC and HIA.

[50] Another model for the origin of mantle anisotropy is that it is caused by present-day mantle flow [*Vinnik et al.*, 1992]. This hypothesis is based on the observation that a significant number of observed fast directions are consistent with the absolute plate motion (APM) direction, although significant differences have been documented. Under the mantle flow assumption, such differences were attributed to small-scale or regionalized mantle flow, as suggested beneath a number of areas such as Tien Shan [*Makeyeva et al.*, 1992], the Baikal rift zone [*Gao et al.*, 1994b, 1997], the Rio Grande Rift [*Sandvol et al.*, 1992], and the western United States [*Savage and Sheehan*, 2000]. In our study area, the fast polarization directions at the eastern stations are almost identical to the movement direction of the Eurasian plate relative to the Pacific plate [*DeMets et al.*, 1990], with a difference of less than 15° and a mean of 7 ± 5° (Figure 1). At the present the Eurasian plate is moving (in a hot spot frame) at a rate of about 2 cm/a toward the direction of about 65° counterclockwise from the north in the study area [*Gripp and Gordon*, 2002], and thus APM is not responsible for either the consistently E-W fast directions observed in the eastern region, or the spatially varying fast directions in the western region.

[51] For the eastern part of the study area, overwhelming geochemical and geophysical data have suggested a thinned lithosphere, with a thickness ranging from 60 to 120 km [*Ma et al.*, 1989; *Griffin et al.*, 1998], leading to a subcrustal lithosphere thickness of 30–90 km. Therefore the lithosphere alone is too thin to produce the observed splitting time, even under the assumption that the crust and the subcrustal lithosphere deform coherently. In addition, if the splitting has a lithospheric origin, one would expect that a thicker lithosphere corresponds to a larger δt. This anticipated relationship is not observed. On the contrary, δt values at stations in the western region, which has thicker subcrustal lithosphere (90–120 km), are significantly smaller than those observed at eastern stations. The large uncertainties and low spatial resolution of the estimated thickness of the lithosphere prevents a more quantitative comparison with the observed splitting times.

[52] Therefore it is unlikely that lithospheric fabrics contribute significantly to the observed splitting times in the eastern region, and consequently, we are left with the options of mantle flow in the MTZ, in the asthenosphere (taken here as the plastic layer between the base of the lithosphere to the 410 km discontinuity), or in the entire zone from the base of the lithosphere to the bottom of the MTZ.

[53] In a "normal" MTZ that is not occupied by subducted slabs, the dominant mineral is wadsleyite (β spinel) in the upper MTZ (410–520 km), and ringwoodite (γ spinel) in the lower MTZ (520–670 km). Numerical modeling and mineral physical experiments suggest that both are incapable of generating significant shear wave splitting for vertically propagating *SKS* phase [*Tommasi et al.*, 2004; *Li et al.*, 2006]. The inferred depth distribution (Figure 13), if it is true, of the source of anisotropy beneath the study area implies that metastable olivine in the subducted slab is mostly responsible for the observed anisotropy. Numerical simulations of olivine-wadsleyite phase transition suggest that the olivine/wadsleyite phase boundary inside a subducting slab can be several hundred kilometers lower than 410 km [*Devaux et al.*, 1997; *Schubert et al.*, 2001]. This model suggests that westward motion (relative to the Eurasian lithosphere) of the subducting Pacific slab in the MTZ causes preferred alignment of the *a* axis of the metastable olivine crystals along the E-W direction with

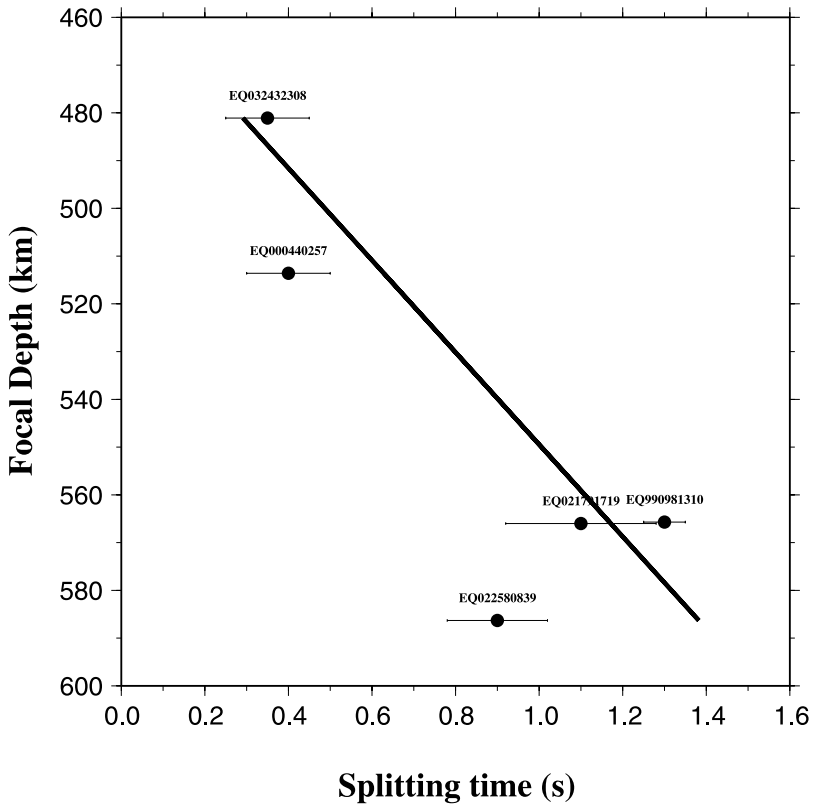

Figure 13. MDJ *S* wave splitting times versus focal depth.

a horizontal foliation plane, and leads to the observed E-W fast directions in the eastern region. The interpretation about the origin of the observed anisotropy is also consistent with the existence of earthquakes as deep as 590 km beneath the study area, which suggests brittle deformation and thus low temperature.

[54] As mentioned in section 5.1, the conclusion that the MTZ contributed to the bulk of the observed splitting times was based on a limited number of local events and could simply reflect lateral variation of seismic anisotropy in the vicinity of station MDJ. If this is the case, east-west asthenospheric flow in the upper mantle might play a major role in the observed anisotropy. Such a mantle flow has recently been suggested beneath the Big Mantle Wedge (BMW) of northeast Asia on the basis of seismic tomographic images and mineral physics experiments, and is thought to be associated with the formation of the Cenozoic basins and basaltic eruptions in our study area [*Zhao et al.*, 2007].

[55] Our results are also consistent with the model that both the asthenospheric flow in the upper mantle and the preferably aligned metastable olivine in the MTZ contribute to the observed anisotropy. Both processes are associated with the westward relative motion of the Pacific plate and thus are expected to generate consistently E-W fast directions.

[56] Finally, the N-S fast directions and the small δt observed at stations near the boundary between western and eastern regions, HHC and HIA, as well as the eastward increase of δt at HIA, can be explained as the results of complex anisotropy under the influence of both mantle flow and fossil lithospheric fabrics.

6. Conclusions

[57] In this study we measured *SKS* splitting parameters at broadband seismic stations in NE China and Mongolia, and used local deep earthquakes to infer the depth of anisotropy. Our preferred model to explain the observed spatial distribution of the splitting parameters and its close correspondence with other observations such as seismic tomographic images, relative plate motion, and distribution of Cenozoic rifted basins and volcanism, is that the observed anisotropy is mostly caused by LPO of crystallographic axes of olivine in the upper mantle portion of the mantle wedge, by LPO of metastable olivine crystals in the subducted Pacific slab in the MTZ, or by a combination of the two. Both processes are associated with the subduction of the deflected Pacific slab. The mantle flow rather than lithospheric deformation model is consistent with the overwhelming geophysical and geochemical evidence that the north China platform has a thin lithosphere due to delamination in the Paleozoic era.

[58] **Acknowledgments.** Data used in the study were archived and managed by CEA and the IRIS DMC. We are grateful to Ray Russo and an anonymous reviewer for constructive suggestions that greatly improved the manuscript. Discussions with Meggie Wen clarified some statistical issues on estimating the errors. The study is funded by the U.S. National Science Foundation under awards EAR 0207466 and EAR 0440320 to K.L. and S.G. Y.G. was partially supported by the Natural Science Foundation of China project 40674021 and Joint Earthquake Science Foundation of China project 102068. This paper is Missouri University of Science and Technology Geology and Geophysics contribution 3.

References

Ai, Y., T. Zheng, W. Xu, Y. He, and D. Dong (2003), A complex 660 km discontinuity beneath northeast China, *Earth Planet. Sci. Lett.*, *212*, 63–71.

Alsina, D., and R. Snieder (1996), Constraints on the velocity structure beneath the Tornquist-Teisseyre zone from beamforming analysis, *Geophys. J. Int.*, *126*, 205–218.

Anderson, M. L., G. Zandt, E. Triep, M. Fouch, and S. Beck (2004), Anisotropy and mantle flow in the Chile-Argentina subduction zone from shear wave splitting analysis, *Geophys. Res. Lett.*, *31*, L23608, doi:10.1029/2004GL020906.

Ando, M., Y. Ishikawa, and F. Yamazaki (1983), Shear wave polarization anisotropy in the upper mantle beneath Honshu, Japan, *J. Geophys. Res.*, *88*, 5850–5864.

Audoine, E., M. K. Savage, and K. Gledhill (2004), Anisotropic structure under a back arc spreading region, the Taupo Volcanic Zone, New Zealand, *J. Geophys. Res.*, *109*, B11305, doi:10.1029/2003JB002932.

Baccheschi, P., L. Margheriti, and M. S. Steckler (2007), Seismic anisotropy reveals focused mantle flow around the Calabrian slab (southern Italy), *Geophys. Res. Lett.*, *34*, L05302, doi:10.1029/2006GL028899.

Bowman, J. R., and M. Ando (1987), Shear-wave splitting in the upper-mantle wedge above the Tonga subduction zone, *Geophys. J. Int.*, *88*, 25–41.

Crampin, S., and D. C. Booth (1985), Shear-wave polarization near the North Anatolia fault. II. Interpretation in terms of crack-induced anisotropy, *Geophys. J. R. Astron. Soc.*, *83*, 75–92.

Darby, B. J., G. A. Davis, and Y. Zheng (2001), Structural evolution of the southwestern Daqing Shan, Yinshan belt, Inner Mongolia, China, *Geol. Soc. Am. Mem.*, *194*, 199–214.

Davis, G. A., Y. Zheng, C. Wang, B. J. Darby, C. Zhang, and G. Gehrels (2001), Mesozoic tectonic evolution of the Yanshan fold and thrust belt, with emphasis on Hebei and Liaoning provinces, northern China, *Geol. Soc. Am. Mem.*, *194*, 171–197.

DeMets, C., R. Gordon, D. Argus, and S. Stein (1990), Current plate motions, *Geophys. J. Int.*, *101*, 425–478.

Devaux, J. P., G. Schubert, and C. Anderson (1997), Formation of a metastable olivine wedge in a descending slab, *J. Geophys. Res.*, *102*, 24,627–24,637.

Fischer, K. M., and D. A. Wiens (1996), The depth distribution of mantle anisotropy beneath the Tonga subduction zone, *Earth Planet. Sci. Lett.*, *142*, 253–260.

Fischer, K. M., M. J. Fouch, D. A. Wiens, and M. S. Boettcher (1998), Anisotropy and flow in Pacific subduction zone back-arcs, *Pure Appl. Geophys.*, *151*, 463–475.

Fouch, M. J., and K. M. Fischer (1996), Mantle anisotropy beneath northwest Pacific subduction zones, *J. Geophys. Res.*, *101*, 15,987–16,002.

Fouch, M. J., and S. Rondenay (2006), Seismic anisotropy beneath stable continental interiors, *Phys. Earth Planet. Inter.*, *158*, 292–320, doi:10.1016/j.pepi.2006.01.022.

Fukao, Y., S. Widiyantoro, and M. Obayashi (2001), Stagnant slabs in the upper and lower mantle transition region, *Rev. Geophys.*, *39*, 291–323.

Galassi, M., J. Davies, J. Theiler, B. Gough, G. Jungman, M. Booth, and F. Rossi (2007), *GNU Scientific Library Reference Manual*, 251 pp., Network Theory Ltd., Bristol, U.K.

Gao, S., P. M. Davis, H. Liu, P. Slack, Y. A. Zorin, N. A. Logatchev, M. Kogan, P. Burkholder, and R. P. Meyer (1994a), Asymmetric upwarp of the Asthenosphere beneath the Baikal Rift zone, Siberia, *J. Geophys. Res.*, *99*, 15,319–15,330.

Gao, S., P. M. Davis, H. Liu, P. D. Slack, Y. A. Zorin, V. V. Mordvinova, V. M. Kozhevnikov, and R. P. Meyer (1994b), Seismic anisotropy and mantle flow beneath the Baikal rift zone, *Nature*, *371*, 149–151.

Gao, S. S., P. M. Davis, K. H. Liu, P. D. Slack, A. W. Rigor, Y. A. Zorin, V. V. Mordvinova, V. M. Kozhevnikov, and N. A. Logatchev (1997), *SKS* splitting beneath continental rift zones, *J. Geophys. Res.*, *102*, 22,781–22,797.

Gilder, S. A., G. R. Keller, M. Luo, and P. C. Goodell (1991), Timing and spatial distribution of rifting in China, *Tectonophysics*, *197*, 225–243.

Griffin, W. L., Z. Andi, S. Y. O'Reilly, and C. G. Ryan (1998), Phanerozoic evolution of the lithosphere beneath the Sino-Korean Craton, in *Mantle Dynamics and Plate Interactions in East Asia*, *Geodyn. Ser.*, vol. 27, edited by J. F. J. Flower et al., pp. 107–126, AGU, Washington, D. C.

Gripp, A. E., and R. G. Gordon (2002), Young tracks of hotspots and current plate velocities, *Geophys. J. Int.*, *150*, 321–364.

He, M. (1990), *1556 Years of Historical Earthquakes in China* (in Chinese), 92 pp., Shaanxi Peoples Publ., Xian, China.

Hsu, K. J., and H. Chen (1999), *Geologic Atlas of China*, 262 pp., Elsevier, New York.

Iidaka, T., and F. L. Niu (2001), Mantle and crust anisotropy in the eastern China region inferred from waveform splitting of *SKS* and *PpSms*, *Earth Planets Space*, *53*, 159–168.

Kroner, A., B. F. Windley, G. Badarch, O. Tomurtogoo, E. Hegner, D. Y. Liu, and M. T. D. Wingate (2005), Accretionary growth in the Central Asian Orogenic Belt of Mongolia during the Neoproterozoic and Palaeozoic and comparison with the Arabian-Nubian Shield and the present southwest Pacific, *Geophys. Res. Abstr.*, *7*, 06650.

Lassak, T. M., M. J. Fouch, C. E. Hall, and E. Kaminski (2006), Seismic characterization of mantle flow in subduction systems: Can we resolve a hydrated mantle wedge?, *Earth Planet. Sci. Lett.*, *243*, 632–649.

Levin, V., W. Menke, and J. Park (1999), Shear wave splitting in the Appalachians and the Urals: A case for multilayered anisotropy, *J. Geophys. Res.*, *104*, 17,975–17,993.

Li, L., D. J. Weidner, J. Brodholt, D. Alfe, and G. D. Price (2006), Elasticity of Mg_2SiO_4 ringwoodite at mantle conditions, *Phys. Earth. Planet. Inter.*, *157*, 181–187.

Liu, H., P. M. Davis, and S. Gao (1995), *SKS* splitting beneath southern California, *Geophys. Res. Lett.*, *22*, 767–770.

Liu, X. Q., H. L. Zhou, H. Li, and A. D. Ji (2001), Anisotropy of the upper mantle in Chinese mainland and its vicinity (in Chinese), *Acta Seismol. Sin.*, *23*, 337–346.

Luo, Y., Z. X. Huang, Y. J. Peng, and Y. J. Zheng (2004), *SKS* wave splitting study of China and adjacent regions (in Chinese), *Chin. J. Geophys.*, *47*, 812–821.

Ma, X., J. Zhang, and Q. Lao (1989), Precambrian tectonic framework, in *Lithospheric Dynamics Atlas of China*, p. 5, China Cartogr. Publ. House, Bejing.

Makeyeva, L. I., L. P. Vinnik, and S. W. Roecker (1992), Shear-wave splitting and small-scale convection in the continental upper mantle, *Nature*, *358*, 144–147.

Marone, F., and B. Romanowicz (2007), The depth distribution of azimuthal anisotropy in the continental upper mantle, *Nature*, *447*, 198–201.

Miller, M. S., B. L. N. Kennett, and A. Gorbatov (2006), Morphology of the distorted subducted Pacific slab beneath the Hokkaido corner, Japan, *Phys. Earth. Planet. Inter.*, *156*, 1–11.

Ozalaybey, S., and W.-P. Chen (1999), Frequency-dependent analysis of *SKS*/*SKKS* waveforms observed in Australia: Evidence for null birefringence, *Phys. Earth. Planet. Inter.*, *114*, 197–210.

Ren, J., Z. Wang, B. Chen, C. Jiang, and B. Niu (1999), *Tectonic Map of China and Adjacent Areas*, Geology Publ. House, Beijing, China.

Ren, J., K. Tamaki, S. Li, and J. Zhang (2002), Late Mesozoic and Cenozoic rifting and its dynamic setting in eastern China and adjacent areas, *Tectonophysics*, *344*, 175–205.

Rumpker, G., and T. Ryberg (2000), New Fresnel-zone estimates for shear-wave splitting observations from finite-difference modeling, *Geophys. Res. Lett.*, *27*, 205–208.

Russo, R. M., and P. G. Silver (1994), Trench-parallel flow beneath the Nazca plate from seismic anisotropy, *Science*, *263*, 1105–1111.

Sandvol, E., and J. Ni (1997), Deep azimuthal seismic anisotropy in the southern Kurile and Japan subduction zones, *J. Geophys. Res.*, *102*, 9911–9922.

Sandvol, E., J. Ni, S. Ozalaybey, and J. Schlue (1992), Shear-wave splitting in the Rio Grande Rift, *Geophys. Res. Lett.*, *19*, 2337–2340.

Savage, M. K. (1999), Seismic anisotropy and mantle deformation: What have we learned from shear wave splitting? Rev, *Geophys.*, *37*, 65–106.

Savage, M. K., and A. F. Sheehan (2000), Seismic anisotropy and mantle flow from the Great Basin to the Great Plains, western United States, *J. Geophys. Res.*, *105*, 13,715–13,734.

Schubert, G., D. L. Turcotte, and P. Olson (2001), *Mantle Convection in the Earth and Planets*, Cambridge Univ. Press, New York.

Shedlock, K. M., S. J. Hellinger, and H. Ye (1985), Evolution of the Xiaoliao Basin, *Tectonics*, *4*, 171–185.

Silver, P. G. (1996), Seismic anisotropy beneath the continents - probing the depths of geology, *Annu. Rev. Earth Planet. Sci.*, *24*, 385–432.

Silver, P. G., and W. W. Chan (1991), Shear wave splitting and subcontinental mantle deformation, *J. Geophys. Res.*, *96*, 16,429–16,454.

Silver, P. G., and M. Savage (1994), The interpretation of shear-wave splitting parameters in the presence of two anisotropic layers, *Geophys. J. Int.*, *119*, 949–963.

Silver, P. G., S. S. Gao, and K. H. Liu (2001), Mantle deformation beneath southern Africa, *Geophys. Res. Lett.*, *28*, 2493–2496.

Smith, G. P., D. A. Wiens, K. M. Fischer, L. M. Dorman, S. C. Webb, and J. A. Hildebrand (2001), A complex pattern of mantle flow in the Lau Backarc, *Science*, *292*, 713–716.

Tommasi, A., D. Mainprice, P. Cordier, C. Thoraval, and H. Couvy (2004), Strain-induced seismic anisotropy of wadsleyite polycrystals and flow patterns in the mantle transition zone, *J. Geophys. Res.*, *109*, B12405, doi:10.1029/2004JB003158.

Vinnik, L. P., L. I. Makeyeva, A. Milev, and A. Y. Usenko (1992), Global patterns of azimuthal anisotropy and deformations in the continental mantle, *Geophys. J. Int.*, *111*, 433–447.

Ye, H., K. M. Shedlock, and S. J. Hellinger (1985), The north China basin: An example of a Cenozoic rifted intraplate basin, *Tectonics*, *4*, 153–169.

Yin, A., and S. Nie (1996), A Phanerozoic palinspastic reconstruction of China and its neighboring regions, in *The Tectonic Evolution of Asia*, edited by A. Yin and T. M. Harrison, pp. 442–485, Cambridge Univ. Press, New York.

Zhang, N. F. (2006), The uncertainty associated with the weighted mean of measurement data, *Metrologia*, *43*, 195–204.

Zhao, L., and T. Zheng (2005), Using shear wave splitting measurements to investigate the upper mantle anisotropy beneath the North China Craton: Distinct variation from east to west, *Geophys. Res. Lett.*, *32*, L10309, doi:10.1029/2005GL022585.

Zhao, D., S. Maruyama, and S. Omori (2007), Mantle dynamics of western Pacific and east Asia: Insight from seismic tomography and mineral physics, *Gondwana Res.*, *11*, 120–131.

Zheng, S., and Y. Gao (1994), Azimuthal anisotropy in lithosphere on the Chinese mainland from observations of *SKS* at CDSN (in Chinese), *Acta Seismol. Sin.*, *16*, 131–140.

S. S. Gao and K. H. Liu, Department of Geological Sciences and Engineering, Missouri University of Science and Technology, Rolla, MO 65409, USA. (sgao@mst.edu; liukh@mst.edu)

Y. Gao and J. Wu, Institute of Earthquake Science, China Earthquake Administration, Beijing 100036, China. (gaoyuan@seis.ac.cn; xianhua123@yahoo.com)